iEnergy

ARTICLE

https://doi.org/10.23919/IEN.2023.0038

Impact of coupled ground wire interference on the precision of electric field sensors

Xinting Liu[1], Shilin Wu[1] ✉, Haoyu Ma[1], Huiquan Zhang[1], Ran Bi[1], Bing Tian[2], Qiancheng Lv[2] and Jun Hu[1] ✉

ABSTRACT

Electric field measurement holds immense significance in various domains. The power supply and signal acquisition units of the sensor may be coupled with ground wire interference, which could result in reduced measurement accuracy. Moreover, this problem is often ignored by researchers. This paper investigated the origin of ground coupling interference in electric field sensors and its impact on measurement accuracy. A miniature undistorted electric field sensor with wireless transmission was compared with existing D-dot, microelectromechanical systems (MEMS), and optical sensors. The results indicate that MEMS and D-dot exhibit diminished accuracy in measuring electric fields under uniform conditions, owing to interference from ground wires. In the case of transmission lines with non-uniform conditions, the wireless sensor exhibited a measurement error of 5%, whereas the optical sensor showed an error rate of approximately 8%. However, the D-dot sensor displayed a measurement error exceeding 50%, whereas the MEMS sensor yielded an error as high as 150%. This means that the wireless sensor isolates the ground-coupled interference signal and realizes the distortion-free measurement of the electric field. The wireless sensors will find extensive applications in new power systems for intelligent equipment status perception, fault warning, and other scenarios.

KEYWORDS

Electric field sensor, coupled ground wire interference, distortion-free measurement.

Electric field measurement holds immense significance in various domains, including power transmission, aerospace engineering, the petrochemical industry, and meteorological detection. In recent years, with the depletion of fossil fuels, there has been an urgent need for clean and low-carbon energy transformation[1]. Large-scale distributed energy will become the main body of new power sources in the power grid and occupy a dominant position in the power structure[2]. With a plethora of clean energy and power electronic equipment connected to the grid, the fundamental characteristics of the future grid are undergoing profound transformations[3]. Real-time measurement feedback and dynamic adjustment of power grid state quantities are required[4]. Electric field information is one of the basic physical quantities of the power system. It contains a large amount of information on the operating status of power grid equipment. Through edge computing, deep learning, and artificial intelligence methods, the intelligent perception of equipment status information and intelligent self-healing of faults can be quickly realized. This provides crucial foundational support for intelligent equipment status perception, deep information fusion, and optimal resource allocation in new power systems[5–7]. Therefore, the accurate measurement of electric field information has become an urgent need for the digital development of new power systems. Figure 1 describes the network of sensors in a smart grid for information perception.

The application of an electric field sensor requires not only a sensor with a wide frequency range and high dynamic range, but also insulation, miniaturization, and the capability for device integration[8,9]. When measuring the electric field, the charge generated by the dielectric on the surface of the electric field sensor usually leads to a certain degree of distortion of the electric field[10]. If a part of the sensor is grounded, it will cause interference from the ground wire into the measurement loop, resulting in a change to the electric field distribution. This can result in significant distortion of the electric field, greatly reducing the accuracy of sensor measurements and posing challenges for large-scale applications.

At present, the miniature electric field sensors commonly used are divided into optical sensors[11,12], mechanical sensors[13,14], D-dot sensors[15], and so on, according to different working principles. The optical sensor converts the electric field signal into an optical signal using energy coupling and the electro-optic effect. It has the characteristics of lossless transmission, a wide measurement frequency range, and a fast dynamic response[16,17]. The optical sensors for high electric field measurements can achieve wide bandwidths of up to 100 MHz and high resolutions of up to 50 V/m. For low-field measurements, the optical sensors can even reach GHz bandwidths and mV/m resolutions[18]. With the rapid development of micro-nano technology, the micro-electric field sensors based on microelectromechanical systems (MEMS) technology have received the attention of researchers. The primary sensing principles utilized by MEMS electric field sensors encompass charge induction, electrostatic force actuation, piezoresistive effect, and other related mechanisms[19,20]. The miniature MEMS electric field sensors boast a resolution of approximately 250 V/m and can measure electric fields up to 2500 V/m, offering exceptional integration, miniaturization, and sensitivity. The D-dot sensor detects electric fields by measuring the rate of change in the electric displacement vector, exhibiting wide frequency bandwidth and minimal dispersion, making it a popular choice for ultra-wideband electromagnetic pulse measurements. Due to its compact size, the sensor is well-suited for measuring confined spaces[21,22].

For the optical sensor, the sensing and measuring modules are connected via optical fiber. The change in refractive index or light

[1]Department of Electrical Engineering, Tsinghua University, Beijing 100084, China; [2]Southern Power Grid Digital Grid Research Institute Co., Ltd., Guangzhou 510663, China

Address correspondence to Shilin Wu, wushilin@tsinghua.edu.cn; Jun Hu, hjun@tsinghua.edu.cn

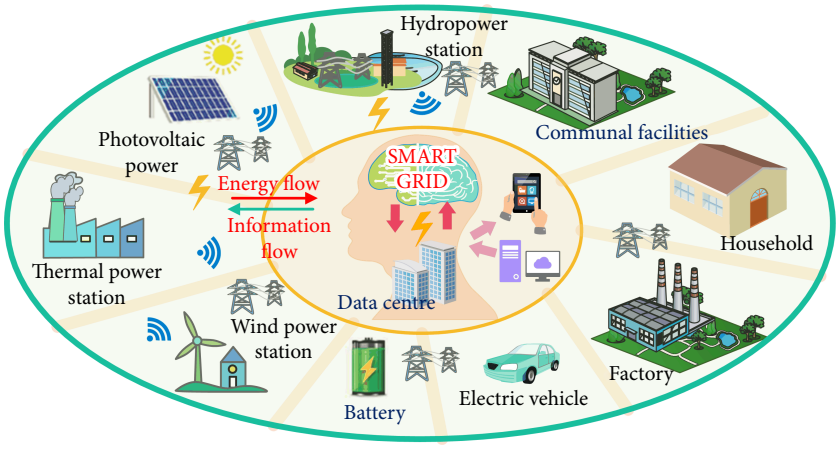

Fig. 1 Sensor network in the smart grid.

intensity reflects the electric field intensity, isolating the electrical signal of the signal acquisition unit and avoiding ground wire coupling interference. This ensures high accuracy in measuring electric fields, which is why most commercial electric field sensors are optical sensors. However, the integration is challenging due to the requirement for a complete set of optical systems, and its measurement accuracy heavily relies on the performance of optical devices while being susceptible to signal offset caused by temperature[23]. As of yet, the optimal solution is currently unavailable. Andreas Kainz et al.[8] developed a MEMS electric field sensor with a movable silicon spring, which operated on the principle of electrostatic coupling. The change in luminous flux caused by the movable silicon block blocking the LED was measured using a photodiode. Since the optical signal isolates the interference of the ground wire, the electric field is undistorted. However, the preparation process is complicated due to the requirement for a complex optical measurement system and the output of the sensor demands high stability of LED. This hinders large-scale development and application, and researchers have not conducted in-depth research on this basis.

For non-optical electric field sensors, such as MEMS and D-dot, the back-end signal conditioning is integrated into the printed circuit board (PCB). The sensing module and measurement module directly convert electrical signals, while electrostatically induced charges are transformed into voltage signals[24]. As the acquisition system solely relies on electrical signals, it is susceptible to ground wire coupling which can interfere with the signal and lead to a reduction in measurement accuracy of the electric field sensor. Currently, a satisfactory solution has not yet been found. Therefore, the majority of current electric field sensors are optical. However, there is a pressing need to develop non-optical alternatives that offer low cost, minimal distortion, and high stability.

Therefore, this paper will concentrate on analyzing the impact of ground wire coupling signals on non-optical electric field sensor measurement accuracy and designing a signal acquisition system for the sensor to achieve distortion-free electric field measurements. The article is organized as follows. Section 1 introduces the sources of error in electric field measurement under coupled interference from ground wires. In Section 2, we establish a standardized calibration platform for electric fields without any intrusion from ground wires and propose a vertical movement calibration method for electric field sensors. In Section 3, we assess the impact of ground coupling signals on the measurement accuracy of electric field sensors under two typical operating conditions: uniform electric fields generated by parallel plates and non-uniform electric fields produced by transmission lines.

1 Analysis of error sources in electric field measurements from coupled ground wires interference

Since the optical sensor can reflect the electric field signal through the refractive index or light intensity information of the optical signal, it can realize the isolation of ground wire interference, and measure the electric field without distortion. However, the difficulty of integrating optical devices and temperature stability is not being resolved[12]. Non-optical electric field sensors may introduce ground wire interference, leading to the reduced measurement accuracy of the electric field. Taking MEMS electric field sensors as an example, we analyzed the primary source of ground interference.

The MEMS electric field sensor system is shown in Figure 2, which mainly includes sensing electrodes, drive modules, signal acquisition and processing modules, and power supply modules. The main sources of ground interference include two parts: power supply and signal acquisition modules. For instance, due to the tiny mechanical deformation of MEMS electric field sensors, the electrical signal derived from displacement signals is typically at microvolt or microampere levels, necessitating a backend operational amplifier device for signal amplification[25, 26]. The utilization of other types of MESM sensors, such as piezoresistive-based MEMS electric field sensors, necessitates the incorporation of supplementary drive modules and consequently requires corresponding drive power[27, 28]. Hence, the power supply of these drive modules and op-amp devices may introduce ground wire interference. To mitigate this issue, it is recommended to utilize a

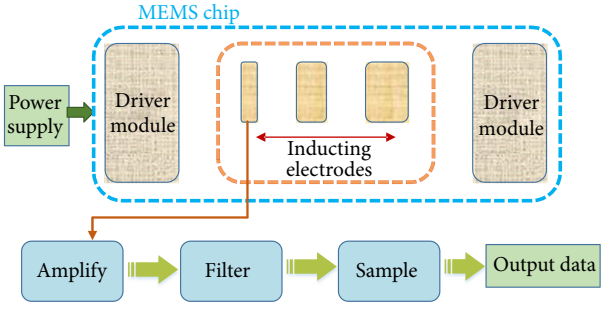

Fig. 2 MEMS electric field sensor system.

floating potential power source such as a battery or an isolation transformer to obtain a stable non-grounded power supply.

The signal acquisition module is another significant source of ground interference, and it is arguably the most critical one. Oscilloscopes are commonly utilized as acquisition instruments for voltage and current signals. However, grounding the acquisition resistance of the oscilloscope may introduce ground wire interference into the electric field measurement circuit, leading to a significant discrepancy between the measured electric field signal and its actual value.

The schematic diagram of the signal acquisition circuit of the electric field sensor is shown in Figure 3, while Figure 3(a) displays an ideal circuit diagram when measuring space electric fields in a non-contact manner. When the output signal of the sensor passes through the signal acquisition system, the circuit can be equivalent to that shown in Figure 3(b). The signal acquisition device can be conceptualized as a parallel circuit model comprising resistors and capacitors. Assuming a uniform electric field, the HV voltage is U_0, and the voltage of the electric field sensor is determined by the voltage division of C_1 and C_2. Ideally, the output signal of the electric field sensor should be independent of the capacitance values of C_1 and C_2. if the sensor's vertical position changes, the magnitudes of C_1 and C_2 will correspondingly vary while maintaining an unchanged output. Consequently, it can be inferred that the sensor achieves distortion-free measurement of the electric field. In other words, the output of the electric field sensor remains constant regardless of vertical displacement within the parallel plate gap.

However, the connection of the signal acquisition device to the measurement circuit results in C_2 being connected in parallel with C_{10} and R_0, leading to a discrepancy between the divided voltage on the sensor and that of the divider, thereby causing a reduction in accuracy for electric field measurements. In addition, when C_1 changes, it will also cause the partial pressure of the measurement circuit to change, which will affect the output value of the electric field sensor. Considering that the impedance of C_2 is significantly higher than that of the acquisition system, it can be inferred that the acquisition system effectively short-circuits the impedance of C_2, thereby introducing a ground wire from the signal acquisition system into the measurement loop. The aforementioned issue significantly diminishes the precision of sensor measurements and renders them inoperable.

To further investigate the impact of ground wire interference on the output accuracy of electric field sensors, a standardized electric field-testing platform was established in this study, and an in-depth analysis was conducted on the effects of ground wire interference on various types of electric field sensors. Moreover, the sensor signal acquisition system is optimized to ensure accurate measurement results without distortion, and a comparative analysis of the performance of different sensors is conducted.

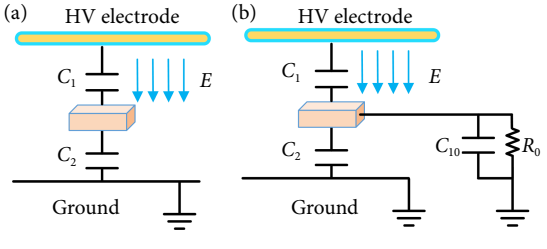

Fig. 3 Schematic diagram of the ground intrusion measurement circuit. **(a)** Ideal circuit diagram, and **(b)** ground intrusion diagram.

2 Experimental equipment and test system without coupled ground wires interference

2.1 Electric field sensors

The MEMS and D-dot electric field sensors used in the research were examined for the influence of ground wire coupling on measurement accuracy, and a solution was proposed to achieve undistorted measurements of electric fields. An electric field sensor with a data wireless transmission system was used. To compare the distortion-free electric field measurement effect, an optical sensor was selected for comparison. The physical map of the electric field sensors is depicted in Figure 4, wherein the optical sensor measures 3 cm × 2 cm × 0.8 cm, the MEMS sensor measures 3 cm × 3 cm × 0.3 cm, the wireless field sensor measures 3 cm × 1.8 cm × 0.8 cm, and the D-dot electric field sensor measures 3 cm × 1.8 cm × 0.6 cm.

The optical sensor, as shown in Figure 4(a), utilizes the Pockels effect to introduce linearly polarized light, generated by the laser source, into the sensor via a polarization-maintaining fiber. Under the influence of the electric field, it is conveyed through a single-mode fiber to an optical detector where it is transformed into an electrical signal that reflects the magnitude of the electric field being measured[29]. The transfer function of the measurement system can be expressed as

$$U_{out} = A\{1 + b\cos[\varphi_0 + \varphi(E)]\} \tag{1}$$

where U_{out} is the electrical signal output by the system; A is the power loss of the optical path and the photoelectric conversion coefficient of the receiver; b is the extinction ratio of the sensor; φ_0 is the static bias point, which is determined by the waveguide structure. $\varphi(E)$ is the phase change caused by the external electric field E, $\varphi(E)=E/E_\pi\pi$, where E_π is the half-wave electric field of the sensor.

The MEMS sensor, as shown in Figure 4(b), is based on the single-layer sidewall sensing principle of Schwarz–Christopher mapping[30]. The single-layer sidewall edge sensing structure undergoes periodic motion due to the shielding electrode, resulting in a periodic exchange of charge between the sensing electrode and sensor substrate. By detecting this periodically exchanged charge, the electric field to be measured is detected:

$$I = 2\omega\varepsilon_0 n_s E A_s \tag{2}$$

where n_s represents the number of sensing capacitors on the single-layer side wall, and A_s is the effective area of the sensing electrode.

The D-dot sensor, as shown in Figure 4(c), is obtained by using a differential parallel capacitor plate. When the electric field

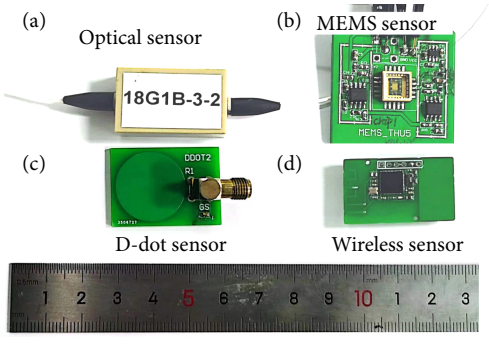

Fig. 4 Four kinds of different electric field sensors. **(a)** Optical sensor, **(b)** MEMS sensor, **(c)** D-dot sensor, and **(d)** wireless sensor.

$E=E_0\sin\omega t$, the electric field signal is obtained by measuring the induced current[24].

$$I = \frac{dQ}{dt} = \omega\varepsilon_0 E_0 \cos\omega t \quad (3)$$

The wireless sensor, as illustrated in Figure 4(d), employs the principle of electrostatic induction for electric field sensing and is applied with a differential structure to mitigate common mode interference. To eliminate interference from ground wires, the previous coaxial cable method has been replaced with wireless data transmission mode.

2.2 Electric field sensor calibration test platform without coupled ground wires interference

The calibration of the electric field sensor has a significant impact on the accuracy of electric field measurements. However, the conventional electric field calibration platform conducts calibration at a fixed position on the planar electrode, disregarding the impact of vertical displacement of the electric field sensor. Therefore, it is crucial to establish a calibration platform that meets the requirements of electric field testing to ensure precise analysis of ground wire intrusion to the electric field sensor. The electric field calibration test platform is shown in Figure 5.

Applying a voltage U on the parallel plate electrodes with a distance of D will generate a uniform electric field E_0, which can be expressed by Eq. (4):

$$E_0 = \frac{U}{D} \quad (4)$$

Due to the limited size of the plate electrode, edge effects are inevitable, resulting in a relative deviation δ between the electric field E_{mid} in the middle of the plate and the theoretical electric field E_0, which can be expressed by Eq. (5):

$$\delta = \frac{E_{mid} - E_0}{E_0} \times 100\% \quad (5)$$

The relative deviation δ is related to the plate diameter L and the electrode gap D. In order to enhance the analysis of electric platform parameters on electric field calibration, we constructed a simulation model of the electric field calibration platform using COMSOL Multiphysics. The parallel plate was configured as a square with a side length (L) of 50 cm, and the gap between the parallel plates (D) was set at 30 cm. The electric field at the edge of the parallel plate is subject to distortion due to the edge effect. To achieve a region with a uniformly distributed electric field, we assume that an area exhibiting an electric field distortion rate within 0.05% can be considered uniform. The sensor output in this region should remain constant as the electric field sensor moves vertically. Simultaneously, we assume that the side length L of the parallel plates remains constant while varying the gap D between them in order to derive the transformation law for the distortion rate of the electric field. Assuming a sensor height variation between 0.6 and 1.5 cm, this study aims to analyze the distribution of errors caused by the vertical movement of the sensor. Through the simulation in COMSOL Multiphysics, Figure 6 illustrates the distribution of the electric field between two parallel electrode plates. The electric field intensity near the plate is amplified by the edge effect, while at the central position, it is slightly attenuated compared to that at the periphery. The change law of relative deviation δ with L/D is shown in Figure 7. It can be seen that as the L/D ratio increases, the relative deviation δ between the electric field E_{mid} at the middle position and the theoretical electric field E_0 is smaller. When the L/D is greater than 1.5, the relative error δ is less than 0.05%. When plate L is 50 cm, D should be less than 33 cm.

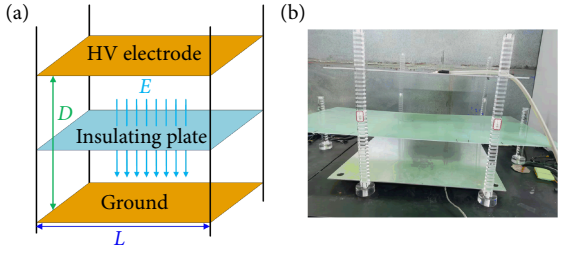

Fig. 5 Electric field calibration test platform. (a) Schematic diagram and **(b)** physical picture.

The electric field sensor is positioned within the gap between the parallel plate electrodes. Due to the presence of the sensor volume, there is a disturbance in the distribution of electric fields, leading to distortion. The impact of this sensor volume (V) on electric field intensity can be expressed by Eq. (6):

$$\delta = \frac{V}{D^3} \times 100\% \quad (6)$$

Since the miniature sensor is small in size and the size does not exceed 1 cm × 2 cm × 3 cm, the plate gap D should be greater than 18 cm. Based on the above factors, the calibration platform L is 50 cm, and the gap D is 30 cm.

Since the sensor is placed in a uniform electric field, the electric force lines will be distorted, resulting in a certain deviation from the true value of the electric field. When moving the sensor along the center line of the plate gap, the electric field distortion near the upper and lower plates is most severe, and the electric field distortion is minimal at the midpoint of the gap. Therefore, we analyzed the distortion of the electric field when the sensor moved an offset distance from the midpoint of the gap. A model was built in

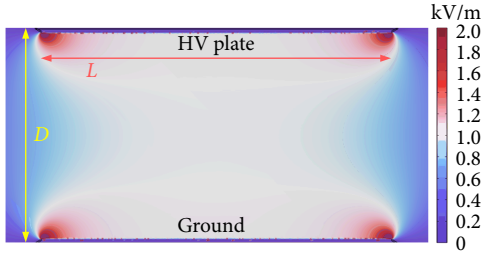

Fig. 6 Electric field distribution between parallel plate electrodes.

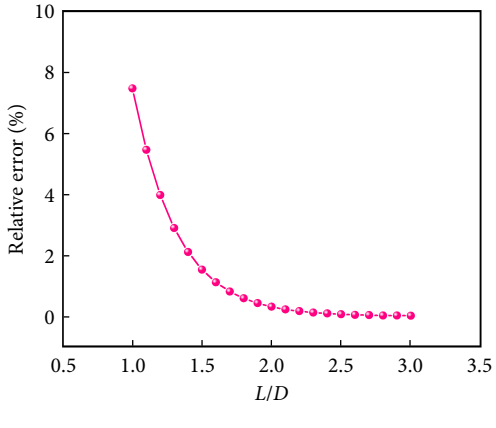

Fig. 7 Variation of relative deviation δ with L/D.

COMSOL Multiphysics for simulation analysis, and the simulation results are shown in Figure 8. It can be observed that when the sensor deviates from the center of the gap, symmetrical distortion arises in the electric field with a greater degree of distortion occurring at a larger offset distance. The relative error remains below 0.1% when the electric field deviates by up to 2 cm from its central position, it can be regarded as a constant electric field. Thus, the electric field sensor can be calibrated within this range of positions.

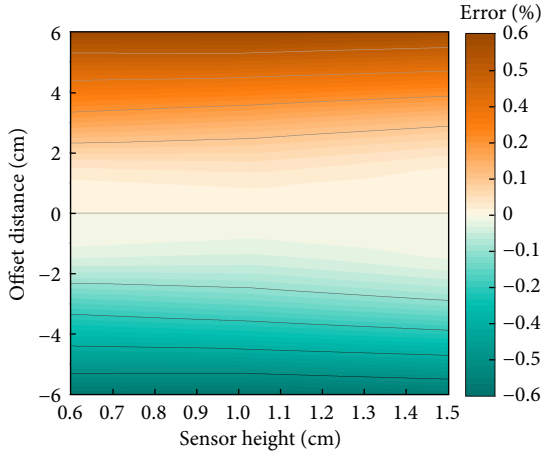

Fig. 8 Error of vertical movement of the sensor.

In summary, to conduct a thorough and precise analysis of the measurement error of an electric field sensor, it is necessary to operate under harsh experimental conditions and perform accuracy testing and error analysis only after meeting the aforementioned requirements.

3 Influence of ground coupling signal on measurement accuracy of electric field sensor

3.1 Uniform electric field under parallel plate electrodes

The first step involved conducting calibration tests on four types of electric field sensors, followed by experiments conducted following the IEEE standard 1308-1994 (R2010). The calibration platform L is 50 cm, and the gap D is 30 cm. The sensor is placed in the middle of the parallel plate gap at d = 15 cm, the voltage signal is applied to the high voltage electrode, and the electric field strength of different amplitudes is obtained according to Eq. (4). According to the simulation results depicted in Figure 8, it can be observed that the electric field within the gap remains constant despite a vertical displacement of 2 cm. Therefore, leveraging on the calibration outcomes obtained at d = 15 cm, which was situated at the midpoint of the parallel plate gap, we proceeded to evaluate and measure electric field values at distances d = 13, 14, 16, and 17 cm from the lower electrode plate.

The optical field sensor's signal was converted from optical fiber to electrical signal by the photoelectric detector and ultimately gathered by an oscilloscope. The signals from both D-dot and MEMS sensors were acquired through coaxial cables and analyzed using oscilloscopes, while the wireless sensor transmitted its signals via Bluetooth.

The measurements of the four electric field sensors are compared and analyzed in Figure 9. It is apparent that there exists a significant dispersion in the electric field measurement obtained by both the D-dot electric field sensor and the MEMS sensor. When the test point (d = 16 and 17 cm) is positioned above the calibration point (d = 15 cm), a larger electric field measurement result is obtained. Conversely, when the test point is below the calibration point, a smaller measurement result is obtained. This indicates that the accuracy of electric field measurements using D-dot and MEMS sensors is affected by the position of the measurement points. For both the optical and wireless sensors, it is evident that the electric field measurements at various positions are nearly identical. This demonstrates that the optical electric field sensor effectively isolates ground signals[31]. As the signal is acquired wirelessly directly from the sensor panel to the receiving end, complete isolation of the ground signal is achieved. This ensures effective separation from ground-coupled signals. Therefore, distortion-free measurement of the electric field can be achieved, enabling accurate determination of the actual electric field value at the centerline position of a uniform parallel plate electrode. Furthermore, measurements taken at different positions yield results consistent with theoretical values.

The electric field measurement errors of the four electric field sensors located at different positions were further analyzed, and the results are depicted in Figure 10. Figure 10(a) illustrates that the D-dot electric field sensor exhibits an error of approximately 6.8% in electric field measurement when the midpoint is offset 1cm in a uniform electric field with a gap of 30 cm. The electric field measurement error increases to about 14.2% when the offset is increased to 2 cm. As the offset distance increases, a larger measurement error will appear, which significantly impacts the accuracy of electric field measurements obtained using this sensor. MEMS electric field sensors, as shown in Figure 10(b), also exhibit a similar pattern. When the gap center is shifted by 1 cm, the electric field measurement error is about 6.4%, and when the gap center is shifted upward by 2 cm, the electric field measurement error is 13.2%. When the center of the gap is shifted downward by 2cm, the electric field measurement error is 11.4%, which shows that the measurement error increases at larger offset distances. This indicates that the presence of a ground wire signal in the measurement unit causes interference when the sensor position is changed, leading to significant measurement inaccuracies. The optical sensor, as shown in Figure 10(c), exhibits negligible electric field measurement error, the measurement error is within 3% and does not increase with offset distance. This indicates that the optical electric field sensor's measurement error is not caused by ground wire interference. The error in the measurement of the optical sensor may be attributed to laser fluctuations or an excessively large half-wave electric field value of the electro-optic crystal. For the wireless sensor, Figure 10(d) demonstrates that the majority of electric field measurement errors are within a 2% range and remain consistent regardless of sensor offset distance. This effectively achieves ground wire interference isolation and results in high-accuracy electric field measurements.

Through the aforementioned analysis, it is evident that the intrusion of the ground wire in MEMS and D-dot sensors leads to a reduction in measurement accuracy. Furthermore, measurements obtained at different positions exhibit varying results; however, they maintain excellent linearity. The results indicate that the calibration coefficient of the electric field is affected by ground wire interference, and the error increases significantly with the distance from the center of the uniform electric field. Even if the sensor has high linearity in calibration, a large error may occur in the actual electric field measurement due to off-center calibration, rendering the calibration result incapable of reflecting the true electric field value. Moreover, when measuring complex non-uniform electric

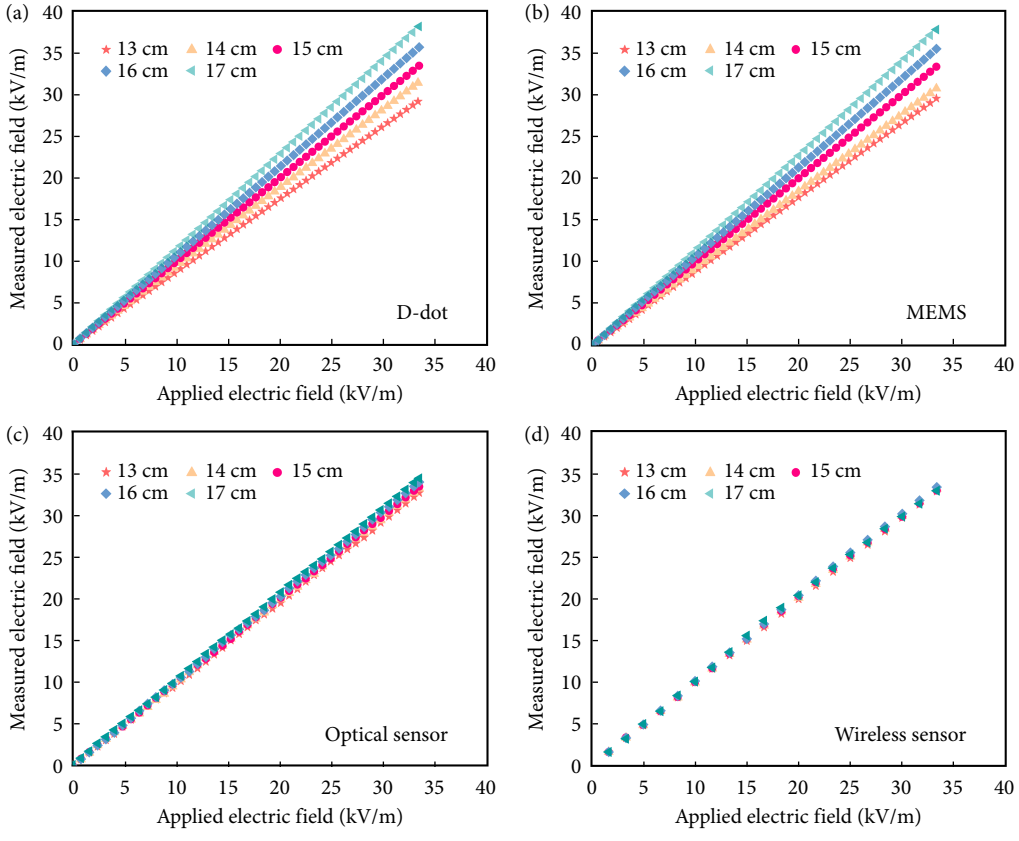

Fig. 9 Electric field measurement results of four electric field sensors. (a) D-dot sensor, **(b)** MEMS sensor, **(c)** optical sensor, and **(d)** wireless sensor.

fields with calibrated sensors, larger measurement errors may arise. Therefore, by optimizing the signal acquisition system, this paper achieved distortion-free measurement of electric fields.

3.2 Non-uniform electric field under transmission line

The interference law of ground for the four sensors under a uniform electric field was analyzed in the front. To further investigate the impact of ground interference on the measurement accuracy of four electric field sensors under complex conditions, this paper employed non-uniform electric field measurements of transmission line conductors to analyze the measurement performance of these sensors in an inhomogeneous electric field environment.

In this paper, a transmission line experimental test platform was constructed, as depicted in Figure 11. The conductors consist of aluminum rods with a radius of 3 cm, which are supported by insulating rods to a height H of 2 m. The sensor is positioned directly below the center of the wire using an adjustable bracket. A power frequency AC voltage is generated through a function generator and high-voltage amplifier. The signal acquisition system for the four sensors is consistent with that used in the calibration platform.

Firstly, an analysis of the electric field distribution beneath the transmission line was conducted. By applying the Gaussian theorem and mirror image method, it can be inferred that the electric field distribution underneath the transmission line conforms to,

$$E(r) = \frac{U}{r\ln\dfrac{2H-a}{a}} \cdot \frac{2H}{2H-a} \tag{7}$$

where U is the applied voltage amplitude, r is the distance from the sensor to the center of the wire, H is the height of the wire, and a is the radius of the wire. It can be seen from Eq. (7) that the electric field distribution beneath the wire is non-uniform, and the comparative analysis of measurement accuracy among the four electric field sensors under such conditions can be conducted.

Based on the previous analysis, the four sensors have been calibrated on a calibration platform and subjected to an electric field distribution test under transmission lines. The results are presented in Figure 12. Figure 12(a) demonstrates that the electric field measurement results of the wireless field sensor are in complete agreement with the theoretical simulation electric field measurement results, indicating excellent measurement accuracy of the sensor. Simultaneously, the measurement outcomes of the optical electric field sensor are in agreement with the values obtained from theoretical simulations. The optical sensor can isolate the interference of ground wire signals and achieve distortion-free measurement of electric fields. Although the wireless sensor optimized in this paper is not composed of all-dielectric materials, it still achieves distortion-free electric field measurements. However, D-dot and MEMS electric field sensors exhibit significant measurement errors. Specifically, the measured value of the D-dot electric field sensor is lower than the theoretical simulation value, while that of the MEMS electric field sensor is higher.

Figure 12(b) depicts a diagram for analyzing measurement errors between the measured values of four sensors and their corresponding theoretical simulation values. It can be observed that the discrepancy between the measured wireless sensor electric field value and theoretical simulation electric field is within 5%, while the optical electric field measurement error is approximately 8%. Possible causes of measurement errors may include the rapid decay of the electric field near the transmission line, which has decreased to less than 1 kV/m at a distance of 40 cm from the center of the wire. This can result in low sensor output and

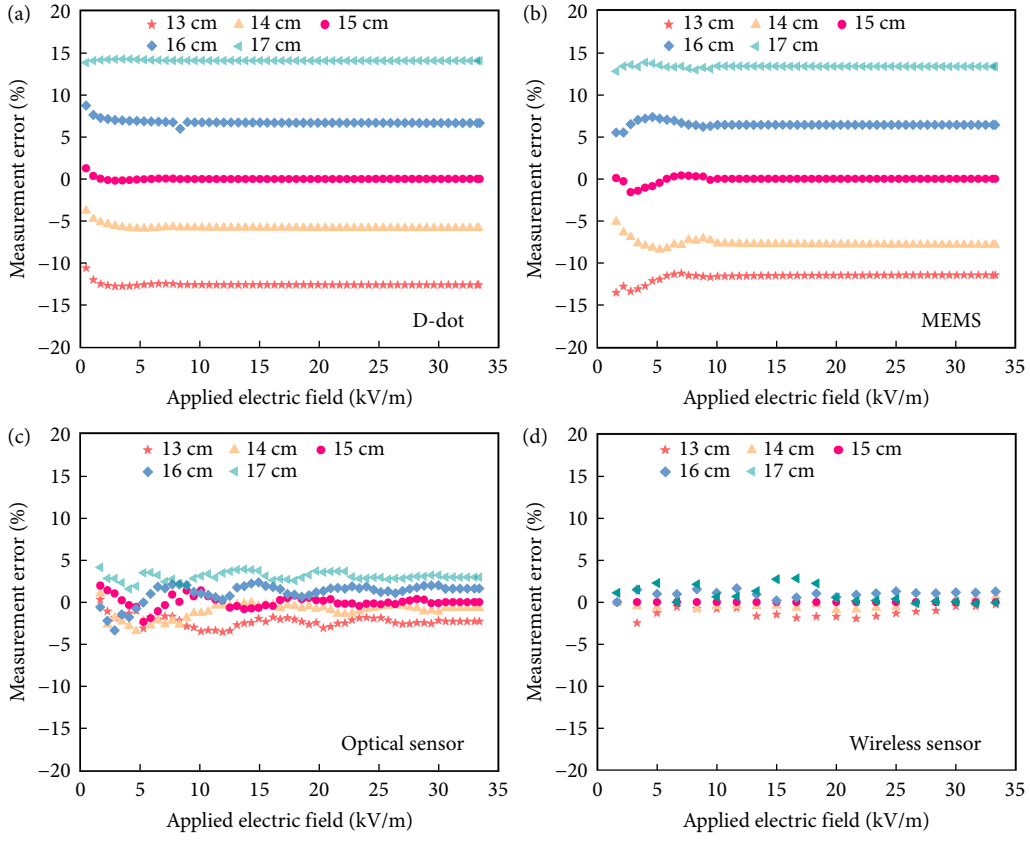

Fig. 10 Analysis of electric field measurement error of four electric field sensors. (a) D-dot sensor, **(b)** MEMS sensor, **(c)** optical sensor, and **(d)** wireless sensor.

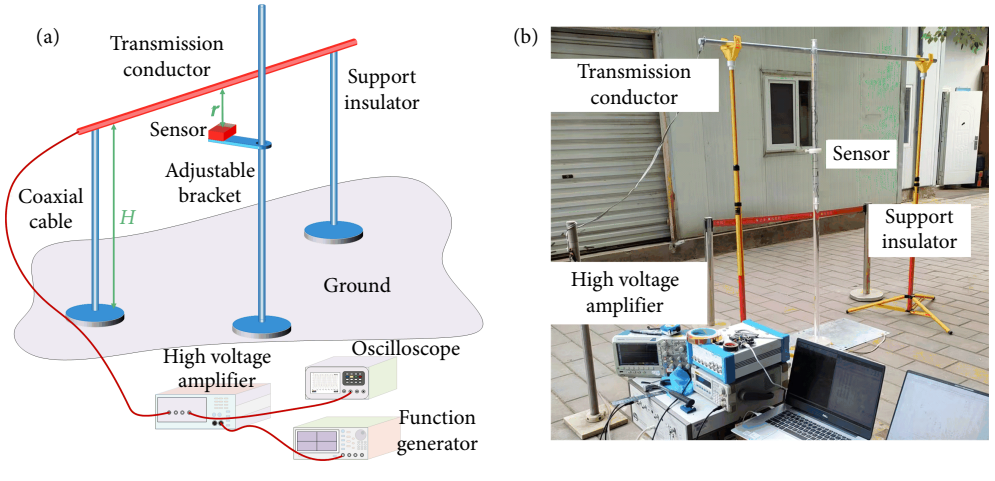

Fig. 11 Experimental diagram of electric field measurement on transmission lines. (a) Schematic diagram and **(b)** physical picture.

potential inaccuracies in measurements within this range. For the D-dot sensor, the electric field measurement error caused by ground wire coupling interference under transmission lines exceeds 50%, while for MEMS sensors, it can be as high as 150%. This indicates that ground interference in a non-uniform electric field can result in significant inaccuracies of the sensor, thereby compromising the ability of an electric field sensor to provide accurate measurements and adversely impacting its overall utility. However, the use of wireless sensors is an effective solution.

4 Conclusions

This paper examined the impact of ground wire coupling interference on electric field sensor measurement accuracy, identified sources of such interference, and analyzed its effects on electric field measurement precision. A miniature electric field sensor of wireless transmission was compared with existing D-dot, MEMS, and optical sensors in terms of performance. The four sensors' performances were analyzed under both uniform electric fields generated by parallel plates and non-uniform electric fields of transmission lines.

(1) In a uniform electric field, the accuracy of electric field measurement by MEMS and D-dot is reduced due to ground wire intrusion, with maximum errors reaching 13.4% and 14.2%, respectively, when the offset center distance is 2 cm. The optical sensor exhibits a measurement error within 5%, whereas the wireless sensor's error is less than 3%. This indicates that ground wire coupling significantly impacts electric field measurement accuracy,

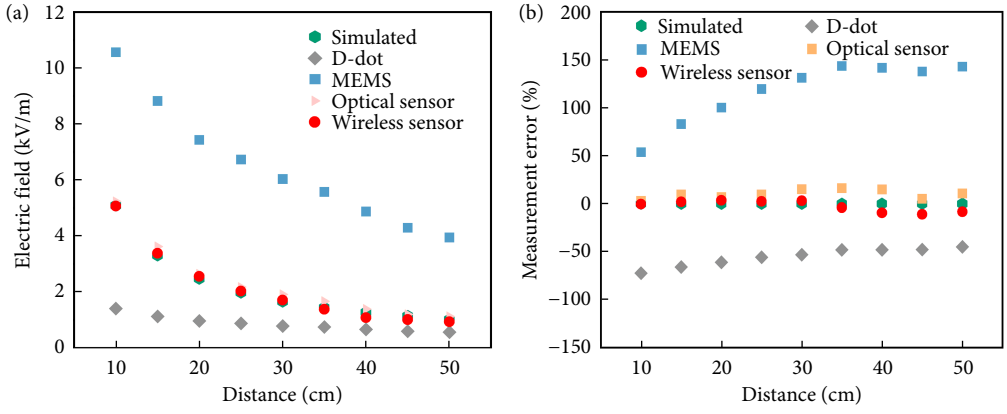

Fig. 12 Electric field distribution test of transmission line. (a) Electric field distribution and **(b)** measurement errors.

and both the optical and wireless sensors can effectively isolate such interference.

(2) In the case of transmission lines, the discrepancy between wireless sensor electric field measurements and theoretical simulation electric field is within 5%, while optical electric field measurement error is approximately 10%. For the D-dot sensor, the measurement error of the electric field under the transmission line exceeds 50%, while that of the MEMS sensor is as high as 150%, indicating that the ground coupling interference signal seriously undermines the measurement accuracy of sensors.

(3) This paper provides a thorough analysis of the impact of ground coupling interference on electric field sensor measurements and demonstrates that our wireless sensor enables accurate measurement without distortion. The measurement accuracy of the wireless sensor surpasses that of optical sensors, and it boasts a small size, low cost, high precision, and distortion-free measurement. It holds great potential in applications such as intelligent equipment status perception and fault warning in new power systems.

Acknowledgements

This work was supported in part by the National Key Research and Development Program of China under Grant 2022YFB3206800 and in part by the National Natural Science Foundation of China under Grant 52125703.

Article history

Received: 18 October 2023; Revised: 22 November 2023; Accepted: 11 December 2023

Additional information

Declaration of competing interest

The authors have no competing interests to declare that are relevant to the content of this article.

References

[1] Wu, S., Zhang, C., Cui, X., Zhang, S., Yang, Q., Shao, T. (2021). Facile synthesis of nitrogen-doped and boron-doped reduced graphene oxide using radio-frequency plasma for supercapacitors. *Journal of Physics D: Applied Physics*, 54: 265501.

[2] He, W., Wu, S., Zhang, Z., Yang, Q. (2022). Vacancy-rich graphene supported electrocatalysts synthesized by radio-frequency plasma for oxygen evolution reaction. *Inorganic Chemistry Frontiers*, 9: 3854–3864.

[3] Strasser, T., Andren, F., Kathan, J., Cecati, C., Buccella, C., Siano, P., Leitao, P., Zhabelova, G., Vyatkin, V., Vrba, P., Marik, V. (2015). A review of architectures and concepts for intelligence in future electric energy systems. *IEEE Transactions on Industrial Electronics*, 62: 2424–2438.

[4] Delle Femine, A., Gallo, D., Landi, C., Lo Schiavo, A., Luiso, M. (2019). Low power contactless voltage sensor for low voltage power systems. *Sensors*, 19: 3513.

[5] Chung, H. E., McMaster, M., Delluomo, A., Vazquez, O., Su, A., Wilson, A. M., Allee, D. R. (2017). Active two-dimensional electric field imaging at very low frequencies. *IEEE Sensors Journal*, 17: 7123–7130.

[6] Takuma, T., Kawamoto, T., Sunaga, Y. (1985). Analysis of calibration arrangements for AC field strength meters. *IEEE Transactions on Power Apparatus and Systems*, PAS-104: 488–496.

[7] Mach, D. M., Koshak, W. J. (2007). General matrix inversion technique for the calibration of electric field sensor arrays on aircraft platforms. *Journal of Atmospheric and Oceanic Technology*, 24: 1576–1587.

[8] Kainz, A., Steiner, H., Schalko, J., Jachimowicz, A., Kohl, F., Stifter, M., Beigelbeck, R., Keplinger, F., Hortschitz, W. (2018). Distortion-free measurement of electric field strength with a MEMS sensor. *Nature Electronics*, 1: 68–73.

[9] Yang, P., Wen, X., Chu, Z., Ni, X., Peng, C. (2021). Non-intrusive DC voltage measurement based on resonant electric field microsensors. *Journal of Micromechanics and Microengineering*, 31: 064001.

[10] Xu, R., Ng, W. C., Zhu, H., Shan, H., Yuan, J. (2012). Equation environment coupling and interference on the electric-field intrabody communication channel. *IEEE Transactions on Biomedical Engineering*, 59: 2051–2059.

[11] Zeng, R., Zhang, Y., Chen, W., Zhang, B. (2008). Measurement of electric field distribution along composite insulators by integrated optical electric field sensor. *IEEE Transactions on Dielectrics and Electrical Insulation*, 15: 302–310.

[12] Yang, Q., Sun, S., He, Y., Han, R. (2019). Intense electric-field optical sensor for broad temperature-range applications based on a piecewise transfer function. *IEEE Transactions on Industrial Electronics*, 66: 1648–1656.

[13] Tant, P., Bolsens, B., Sels, T., Van Dommelen, D., Driesen, J., Belmans, R. (2007). Design and application of a field mill as a high-voltage DC meter. *IEEE Transactions on Instrumentation and Measurement*, 56: 1459–1464.

[14] Krakover, N., Ilic, B. R., Krylov, S. (2022). Micromechanical resonant cantilever sensors actuated by fringing electrostatic fields. *Journal of Micromechanics and Microengineering*, 32: 054001.

[15] Wang, K., Duan, Y., Shi, L., Qiu, S. (2019). Laboratory calibration of D-dot sensor based on system identification method. *Sensors*, 19: 3255.
[16] Yang, Q., Sun, S., Han, R., Sima, W., Liu, T. (2015). Intense transient electric field sensor based on the electro-optic effect of $LiNbO_3$. *AIP Advances*, 5: 107130.
[17] Zhang, Z., Wu, S., He, W., Yang, Q. (2023). A novel transient electric field measurement for low kerr constant liquid dielectrics based on concave spherical mirror conjugate structure. *IEEE Transactions on Instrumentation and Measurement*, 72: 1500308.
[18] Luo, M., Yang, Q., Dong, F., Chen, N., Liao, W. (2022). Miniature micro-ring resonator sensor with electro-optic polymer cladding for wide-band electric field measurement. *Journal of Lightwave Technology*, 40: 2577–2584.
[19] Xue, F., Hu, J., Guo, Y., Han, G., Ouyang, Y., Wang, S. X., He, J. (2020). Piezoelectric–piezoresistive coupling MEMS sensors for measurement of electric fields of broad bandwidth and large dynamic range. *IEEE Transactions on Industrial Electronics*, 67: 551–559.
[20] Han, Z., Xue, F., Hu, J., He, J. (2021). Micro electric field sensors: Principles and applications. *IEEE Industrial Electronics Magazine*, 15: 35–42.
[21] Al Agry, A., Schill, R. A. (2014). Calibration of electromagnetic dot sensor—Part 2: D-dot mode. *IEEE Sensors Journal*, 14: 3111–3118.
[22] Wang, J., Yan, X., Zhong, L., Zhu, X. (2019). Simulation and test of a contactless voltage measurement method for overhead lines based on reconstruction of integral node parameters. *Sensors*, 20: 246.
[23] Sima, W., Han, R., Yang, Q., Sun, S., Liu, T. (2017). Dual $LiNbO_3$ crystal-based batteryless and contactless optical transient overvoltage sensor for overhead transmission line and substation applications. *IEEE Transactions on Industrial Electronics*, 64: 7323–7332.
[24] Huang, F., Yan, Y., Chen, J., Liu, Z., Wang, B. (2019). Calibration uncertainty evaluationof D-dot sensors. *Progress In Electromagnetics Research Letters*, 83: 115–122.
[25] Han, Z., Xue, F., Hu, J., He, J. (2022). Trampoline-shaped micro electric-field sensor for AC/DC high electric field measurement. *IEEE Transactions on Industrial Electronics*, 69: 13791–13798.
[26] Han, Z., Xue, F., Yang, G., Yu, Z., Hu, J., He, J. (2021). Micro-cantilever capacitive sensor for high-resolution measurement of electric fields. *IEEE Sensors Journal*, 21: 4317–4324.
[27] Yu, Z., Chen, S., Mou, Y., Hu, F. (2022). Electrostatic-fluid-structure 3D numerical simulation of a MEMS electrostatic comb resonator. *Sensors*, 22: 1056.
[28] Liu, X., Wang, Z., Wu, Z., Gao, Y., Peng, S., Ren, R., Zheng, F., Lv, Y., Yang, P., Wen, X., Xia, S., Peng, C. (2021). Enhanced sensitivity and stability of a novel resonant MEMS electric field sensor based on closed-loop feedback. *IEEE Sensors Journal*, 21: 22536–22543.
[29] Zeng, R., Wang, B., Niu, B., Yu, Z. (2012). Development and application of integrated optical sensors for intense E-field measurement. *Sensors*, 12: 11406–11434.
[30] Mou, Y., Yu, Z., Huang, K., Ma, Q., Zeng, R., Wang, Z. (2018). Research on a novel MEMS sensor for spatial DC electric field measurements in an ion flows field. *Sensors*, 18: 1740.
[31] Zhu, T., Zhou, L., Liu, M., Zhang, J., Shi, L. (2015). High sensitive space electric field sensing based on micro fiber interferometer with field force driven gold nanofilm. *Scientific Reports*, 5: 15802.